

# Ratiometric and reusable fluorescent nanoparticles for $\text{Zn}^{2+}$ and $\text{H}_2\text{PO}_4^-$ detection in aqueous solution and living cells†

Chunsheng He, Weiping Zhu,\* Yufang Xu, Ye Zhong, Juan Zhou and Xuhong Qian\*

Received 17th June 2010, Accepted 7th September 2010

DOI: 10.1039/c0jm01925a

In this work, three kinds of core-shell silica nanoparticle-based fluorescent materials were prepared based on a modified Stöber–Van Blaaderen method. They were characterized by transmission electron microscopy (TEM), scanning electron microscopy (SEM), dynamic light scattering (DLS), FT-IR, and several other spectroscopic methods. Firstly, The silica@sensor-1 nanoparticle (SSN) showed high selectivity toward  $\text{Zn}^{2+}$ , which can detect  $\text{Zn}^{2+}$  in aqueous solution and living cells. It also can be reused to detect  $\text{Zn}^{2+}$  for at least four cycles after a simple regeneration. Secondly, to create a ratiometric measurement platform, the dye-2@silica nanoparticles (DSN), a new class of core-shell fluorescent silica nanoparticles were prepared with an acenaphtho[1, 2-b]pyrrol-9-carbonitrile chromophore derivative as the inner reference. It showed negligible sensing properties towards  $\text{Zn}^{2+}$ , and the fluorescent intensity was not subjected to interference induced by pH change. Thirdly, the dye-2@silica@sensor-1 nanoparticles (DSSN), with the above reference dye buried inside the silica matrix and a layer of chemosensors anchored onto the surface of silica nanoparticles were prepared. DSSN showed not only the same sensing ability as SSN, but also a clear ratiometric fluorescent signal toward  $\text{Zn}^{2+}$  in aqueous solutions and living cells. On the other hand,  $\text{H}_2\text{PO}_4^-$  is a well-known  $\text{Zn}^{2+}$  binder, so the [DSSN@ $\text{Zn}^{2+}$ ] complex was found to ratiometrically detect  $\text{H}_2\text{PO}_4^-$ . It responded to  $\text{H}_2\text{PO}_4^-$  at a neutral aqueous solution with a detection limit lower than  $6 \times 10^{-6}$  M. Moreover, the ratio of fluorescence intensity was linearly increased in the range 6~500  $\mu\text{M}$  of  $\text{H}_2\text{PO}_4^-$ , which implies a potential application for the quantitation of  $\text{H}_2\text{PO}_4^-$  in aqueous solution. To the best of our knowledge, this is the first example of core-shell silica nanoparticle-based fluorescent materials that can be repeatedly used to ratiometrically detect  $\text{Zn}^{2+}$  and  $\text{H}_2\text{PO}_4^-$  in 100% neutral aqueous solutions.

## Introduction

Fluorescence chemosensors, composed of a substrate binding unit and one or more photoactive components, can signal the presence of selected substrates by the variation in their fluorescence emissions (fluorescence intensity quenching or enhancement, ratiometric measurements).<sup>1</sup> Such systems can be used to measure analyte concentration with high selectivity, rapid response rate and excellent spatial resolution.<sup>2</sup> Therefore, they have drawn considerable attention in the intracellular monitoring of selected species in biological applications. Ratiometric fluorescent sensors measure the changes in the ratio of the signal intensities, which increase the dynamic range and provide a built-in correction for environmental effects.<sup>3</sup>

In the last few years, fluorescent nanomaterials such as metallic nanoparticles (Au and Ag),<sup>4</sup> quantum dots (QDs),<sup>5</sup> lanthanide nanoparticles,<sup>6</sup> and silica nanoparticles<sup>7</sup> have been used as the matrix of various chemosensors. Among such material platforms, silica is “generally recognized as safe” (GRAS) by the US Food and Drug Administration (FDA), and is an attractive support for many applications because of its good

biocompatibility, simple synthetic procedure and relative inertness in many environments.<sup>8</sup> Compared with a single dye molecule, dye-doped silica nanoparticles produce a highly amplified optical signal by bearing a large number of dye molecules in a single silica particle, which can provide a great improvement in sensitivity. Such a silica matrix provides a barrier keeping the dye from its surrounding environment. Both photobleaching and photodegradation that often affect conventional dyes can be minimized. And the flexible silane chemistry also provides versatile routes for the modification of the silica surface. Therefore, fluorescent silica nanoparticles exhibit considerable advantages over conventional molecular dyes in the design of fluorescent labeling agents and chemosensors.<sup>9</sup> Meanwhile, silica-based multifunctional nanoparticles have demonstrated their capability in a wide range of applications, such as early-stage cancer diagnosis,<sup>10</sup> drug delivery,<sup>11</sup> pathogen detection<sup>12</sup> and gene delivery.<sup>13</sup>

There are two methods for the synthesis of organic-dye-doped silica nanoparticles; one is the Stöber method,<sup>14</sup> and the other is the reverse microemulsion method.<sup>15</sup> By either method, one can get multifunctional systems with exquisite shape and size control. Among these architectures, some authors have proposed multistep synthesis of core-shell structures.<sup>16,17</sup> In such nanostructured particle systems, silica could be a scaffold for the template or core-shell of another material. Around this core-shell, some functional molecules can be deposited.<sup>18</sup>

Shanghai Key Laboratory of Chemical Biology, School of Pharmacy East China University of Science and Technology, 130 Meilong Road, Shanghai, 200237, PR China. E-mail: wpzhu@ecust.edu.cn; xhqian@ecust.edu.cn; Fax: (+86) 21-64252603

† Electronic Supplementary Information (ESI) available: Fig. S1–S9, Table 1. See DOI: 10.1039/c0jm01925a/

Recently, silica nanoparticles have been investigated as the matrix of chemosensors, and most of them are used for the detection of the fluorescence quenching species, such as molecular oxygen<sup>19</sup> and  $\text{Cu}^{2+}$ ,<sup>20</sup>  $\text{Pb}^{2+}$ <sup>17</sup> ions. Reports on the elaboration of optical silica nanoparticles chemically bound with fluorophores, especially with the enhancement of the fluorescence intensity for  $\text{Zn}^{2+}$ , are quite scarce.<sup>21,22</sup> Moreover, only one of them showed practical applications in biological systems.<sup>22</sup> In contrast to the common applications in homogeneous solutions, such silica-based fluorescent sensors have the potential for regeneration after simple post-processing, which could be used to construct photoluminescent devices.<sup>23</sup>

Considering the important roles of zinc in various biological processes such as gene transcription, metalloenzyme regulation, neural signal transmission,<sup>24</sup> we have focused on the fabrication of core-shell dye-doped silica nanoparticles as a fluorescent chemosensor for  $\text{Zn}^{2+}$ , by covalently linking the modified sensor **1** to the silica network. In this paper, we prepared monodisperse silica-rich core and sensor-rich shell nanoparticles (silica@sensor-1, SSN), as “off-on” fluorescent chemosensors for  $\text{Zn}^{2+}$  with a high selectivity in aqueous solution and living cells (Fig. 1-i: SSN). To create a ratiometric measurement platform, the dye-2@silica@sensor-1 nanoparticles (DSSN) were prepared with an 8-oxo-8H-acenaphtho[1,2-b]pyrrol-9-carbonitrile derivative as the inner reference-rich core and sensor **1** as a sensor-rich shell (Fig. 1-i: DSSN). Furthermore, it is well known that phosphate ions and their derivatives play important roles in signal transduction and energy storage in biological systems.<sup>25</sup> Some fluorescent and/or colorimetric sensors for  $\text{H}_2\text{PO}_4^-$  have been reported during the past few years.<sup>26,27</sup> To date, there is no report about the fluorescent sensor for  $\text{H}_2\text{PO}_4^-$  in micromolar concentrations in neutral aqueous solutions. To increase the detection limit of  $\text{H}_2\text{PO}_4^-$ , the [DSSN@ $\text{Zn}^{2+}$ ] complex was also prepared as a ratiometric fluorescent sensor for  $\text{H}_2\text{PO}_4^-$  in 100% aqueous solution (Scheme 1).

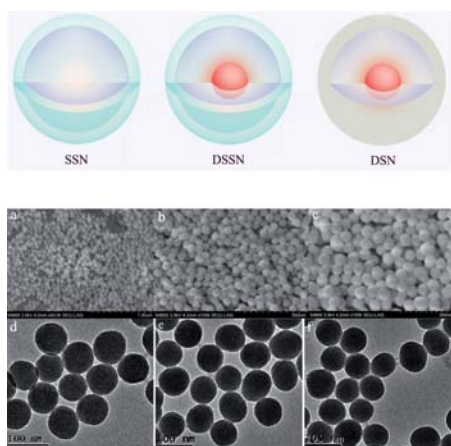
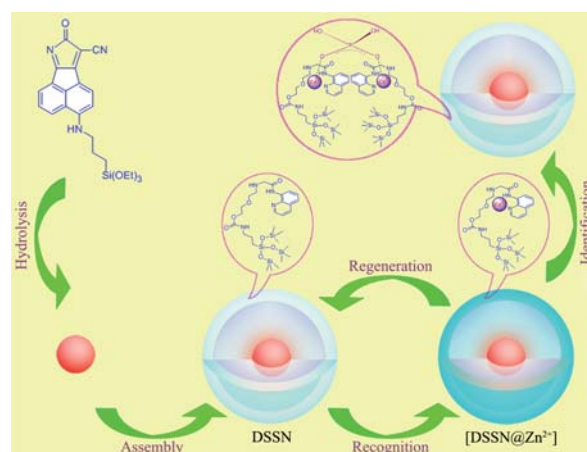


**Fig. 1** (i) Schematic diagrams of three different core-shell architecture fluorescent silica nanoparticles. (ii) (a, d): SEM and TEM images of SSN; (b, e): SEM and TEM images of DSSN; (c, f): SEM and TEM images of DSN.



**Scheme 1** Preparation, recognition (identification) and regeneration of dye-2@sensor-1 core-shell silica nanoparticles (DSSN) for ratiometric fluorescence detecting  $\text{Zn}^{2+}$  and  $\text{H}_2\text{PO}_4^-$ .

## Experimental

### General procedures

All the solvents were of analytical grades without further purification unless otherwise noted.  $^1\text{H-NMR}$  spectra were measured on a Bruker AV-400 spectrometer with chemical shifts reported in ppm (in  $\text{CDCl}_3$ , TMS as internal standard). Electrospray ionization (ESI) mass spectrometry was performed in a HP 1100 LC-MS spectrometer. Melting points were determined by an X-6 micro-melting point apparatus and were uncorrected. All pH measurements were made with a Sartorius basic pH-Meter PB-20. Fluorescence spectra were determined using a Varian Cary Eclipse fluorescence spectrometer. Absorption spectra were determined by a Varian Cary 100 UV-vis spectrophotometer. Fluorescence quantum yields were determined by using quinine sulfate in 0.05 M  $\text{H}_2\text{SO}_4$  ( $\Phi = 0.564$ ) as a reference.

SEM images of the particles were taken by Hitachi S-520 scanning electron microscopy to assess the particle size and shape. To prepare the samples for SEM studies, fluorescent silica nanoparticles were dispersed in water, and the resulting suspension was vortexed and sonicated for 2 min. A drop (1–10  $\mu\text{L}$ ) of the particles suspension was then placed on a piece of a microglass slide and dried overnight in a desiccator.

Dynamic light scattering (DLS) measurements were performed by an ALV/CGS-5022F from ALV Ltd. (German). Hydrodynamic particle diameters were obtained from cumulant fits of the autocorrelation functions at  $90^\circ$  scattering angle.

TEM images of the particles were obtained with a JEM-2100 transmission electron microscope operating at 200 keV. Samples for TEM were prepared by spreading a drop of the nanoparticle solution in ethanol onto standard carbon coated copper grids (200 mesh). Dimensional analysis of nanoparticles from TEM images were performed with the Digital Micrograph software.

FT-IR spectra ( $4000\sim 500\text{ cm}^{-1}$ ) in KBr were collected on a Nicolet NEXUS 470 FT-IR spectrometer. The fluorescent silica nanoparticles were mixed with KBr and pressed to a thin disc for FT-IR detection.

Confocal Microscopy images were obtained using a Nikon A1R spectral confocal microscope. Fluorescence imaging was

performed with a Leica DMIRB with Xenon lamp. Blue emission was collected with a 430~510 nm window, and red emission was collected with a 570~650 nm window.

### Synthesis of fluoroionophore 1

Organic fluorescent sensor **1c** was prepared according to the reported procedure.<sup>28</sup> The modified fluoroionophore **1** was prepared as follows: compound **1c** (145 mg, 0.5 mmol) and triethoxy(3-isocyanatopropyl)silane (148 mg, 0.6 mmol) were dissolved in anhydrous THF (10 mL) with 2–5 drops of Et<sub>3</sub>N under nitrogen atmosphere. The yellow solution was stirred for 48 h under reflux; then the solvent was removed by rotary evaporation and the residue was directly purified by flash column chromatography (silica gel, CH<sub>2</sub>Cl<sub>2</sub>/CH<sub>3</sub>OH = 40/1, v/v) to provide **1** (229 mg, yield 85.2%) as the yellow oil. <sup>1</sup>H (400 MHz, CDCl<sub>3</sub>, 25 °C): δ = 10.44 (–NHCO–, s, 1H), 8.82 (t, *J*<sub>1</sub> = *J*<sub>2</sub> = 2.1 Hz, 1H), 8.81 (t, *J*<sub>1</sub> = *J*<sub>2</sub> = 3.2 Hz, 1H), 8.14 (dd, *J*<sub>1</sub> = 9.6 Hz, *J*<sub>2</sub> = 1.6 Hz, 1H), 7.51 (t, *J*<sub>1</sub> = *J*<sub>2</sub> = 2.4 Hz, 2H), 7.42 (dd, *J*<sub>1</sub> = 6.2 Hz, *J*<sub>2</sub> = 6.0 Hz, 1H), 4.25 (–COCH<sub>2</sub>–, s, 2H), 3.78 (–OCH<sub>2</sub>CH<sub>3</sub>, m, 6H), 3.72–3.68 (–OCH<sub>2</sub>CH<sub>2</sub>O–, m, 4H), 3.62 (–NHCH<sub>2</sub>CH<sub>2</sub>O–, t, *J*<sub>1</sub> = *J*<sub>2</sub> = 4.8 Hz, 2H), 3.56 (–NHCH<sub>2</sub>CH<sub>2</sub>O–, t, *J*<sub>1</sub> = *J*<sub>2</sub> = 3.2 Hz, 2H), 3.31–3.26 (–CH<sub>2</sub>CH<sub>2</sub>CH<sub>2</sub>Si–, m, 2H), 1.72–1.65 (–CH<sub>2</sub>CH<sub>2</sub>CH<sub>2</sub>Si–, m, 2H), 1.19 (–OCH<sub>2</sub>CH<sub>3</sub>, t, *J*<sub>1</sub> = *J*<sub>2</sub> = 7.0 Hz, 9H), 0.67 (–CH<sub>2</sub>CH<sub>2</sub>CH<sub>2</sub>Si–, t, *J*<sub>1</sub> = *J*<sub>2</sub> = 8.2 Hz, 2H). IR(KBr): 3335, 2928, 1639, 1536, 1371, 1250, 1077, 947, 792 cm<sup>–1</sup>. HRMS (EI): [M + H<sup>+</sup>] calcd for C<sub>25</sub>H<sub>41</sub>N<sub>4</sub>O<sub>7</sub>Si, 537.2745; found, 537.2740 (100%).

### Synthesis of fluoroionophore 2

The precursor **2c** was prepared according to the reported procedure.<sup>29</sup> The fluoroionophore **2** was prepared as follows: compound **2c** (200 mg, 0.869 mmol) and 3-aminopropyltriethoxy silane (770 mg, 3.47 mmol) were dissolved in acetonitrile (25 mL) under nitrogen atmosphere. The yellow solution was stirred for 48 h at room temperature; then the solvent was removed by rotary evaporation and the residue was directly purified by flash column chromatography (silica gel, CH<sub>2</sub>Cl<sub>2</sub>/CH<sub>3</sub>OH = 80/1, v/v) to provide **1** (58.9 mg, 15.1%) as the red powder. m.p. > 300 °C. <sup>1</sup>H (400 MHz, CDCl<sub>3</sub>, 25 °C): δ = 8.74 (d, *J* = 7.6 Hz, 1H), 8.44 (d, *J* = 8.4 Hz, 1H), 8.05 (d, *J* = 8.4 Hz, 1H), 7.82 (t, *J*<sub>1</sub> = *J*<sub>2</sub> = 7.6 Hz, 1H), 6.78 (d, *J* = 8.8 Hz, 1H), 3.92 (–OCH<sub>2</sub>CH<sub>3</sub>, q, 6H), 3.76 (–CH<sub>2</sub>CH<sub>2</sub>CH<sub>2</sub>Si–, t, *J*<sub>1</sub> = *J*<sub>2</sub> = 7.2 Hz, 2H), 2.06 (–CH<sub>2</sub>CH<sub>2</sub>CH<sub>2</sub>Si–, t, *J*<sub>1</sub> = *J*<sub>2</sub> = 6.4 Hz, 2H), 0.87 (–CH<sub>2</sub>CH<sub>2</sub>CH<sub>2</sub>Si–, t, *J*<sub>1</sub> = *J*<sub>2</sub> = 7.2 Hz, 2H). IR(KBr): 3297, 2966, 2419, 1727, 1567, 1521, 1451, 1333, 1274, 1192, 1080, 951, 779 cm<sup>–1</sup>. HRMS (EI): [M + H<sup>+</sup>] calcd for C<sub>24</sub>H<sub>28</sub>N<sub>3</sub>O<sub>4</sub>Si, 450.1849; found, 450.1854 (100%).

### Preparation of the core-shell silica@sensor-1 nanoparticles (SSN)

For the preparation of core-shell silica-sensor-1 silica nanoparticles, TEOS (150 μL, 0.405 mmol) and ammonia (0.9 mL, 25% water solution) were added to 25 mL of ethanol in a 313 K thermostated vessel. The reaction mixture was vigorously stirred for 5 h, and then a second amount of TEOS (150 μL, 0.405 mmol) and a second amount of ammonia (0.9 mL, 25% water

solution) were added. The reaction mixture was stirred for another 5 h (DLS analysis yielded a diameter of 64 ± 8 nm for the resulting silica cores). Fluorescent sensor **1** (25.0 mg, 46.7 μmol), TEOS (150 μL, 0.405 mmol), and ammonia (0.4 mL, 25% water solution) were subsequently added, and the mixture was stirred at 313 K for an additional 20 h. After hydrolysis, the nanoparticles were washed extensively with 70% ethyl alcohol and water until the UV/Vis spectrum of the filtrate showed the absence of sensor-**1** absorption. And they were stored in water at 4 °C for future use (DLS analysis yielded a diameter of 80 ± 7 nm for the resulting silica@sensor-1 core-shell nanoparticles).

### Preparation of the core-shell dye-2@silica nanoparticles (DSN)

For the preparation of core-shell dye-2@silica nanoparticles, the aforementioned dye-2 precursor, usually containing around 2.35 × 10<sup>–5</sup> M of dye-2, with TEOS (150 μL, 0.405 mmol) and ammonia (0.9 mL, 25% water solution) were added to 25 mL of ethanol in a 313 K thermostated vessel. The reaction mixture was vigorously stirred for 5 h, and then a second amount of TEOS (150 μL, 0.405 mmol) and a second amount of ammonia (0.9 mL, 25% water solution) were added. The reaction mixture was stirred for another 5 h. After that, TEOS (150 μL, 0.405 mmol), and ammonia (0.4 mL, 25% water solution) were subsequently added, and the mixture was stirred at 313 K for an additional 20 h. After hydrolysis, the nanoparticles were washed extensively with 70% ethyl alcohol and water until the UV/Vis spectrum of the filtrate showed the absence of dye-2 absorption, and they were stored in water at 4 °C for future use.

### Preparation of the core-shell dye-2@sensor-1 nanoparticles (DSSN)

For the preparation of nanoparticles with a compact dye-2 core, the aforementioned dye-2 precursor, usually containing around 2.35 × 10<sup>–5</sup> M of dye-2, with TEOS (150 μL, 0.405 mmol) and ammonia (0.9 mL, 25% water solution) were added to 25 mL of ethanol in a 313 K thermostated vessel. The reaction mixture was vigorously stirred for 5 h, and then a second amount of TEOS (150 μL, 0.405 mmol) and a second amount of ammonia (0.9 mL, 25% water solution) were added. The reaction mixture was stirred for another 5 h (DLS analysis yielded a diameter of 65 ± 7 nm for the resulting dye-2 cores). Fluorescent sensor **1** (25.0 mg, 46.7 μmol), TEOS (150 μL, 0.405 mmol), and ammonia (0.4 mL, 25% water solution) were subsequently added, and the mixture was stirred at 313 K for an additional 20 h. After hydrolysis, the nanoparticles were washed extensively with 70% ethyl alcohol and water until the UV/Vis spectrum of the filtrate showed the absence of dye-2 and sensor-**1** absorption. And they were stored in water at 4 °C for future use (DLS analysis yielded a diameter of 82 ± 5 nm for the resulting dye-2@sensor-1 core-shell nanoparticles).

### Spectrophotometric titrations

The metal salts employed are Hg(ClO<sub>4</sub>)<sub>2</sub>·3H<sub>2</sub>O, Cd(ClO<sub>4</sub>)<sub>2</sub>·6H<sub>2</sub>O, Pb(ClO<sub>4</sub>)<sub>2</sub>·3H<sub>2</sub>O, AgClO<sub>4</sub>·H<sub>2</sub>O, Zn(ClO<sub>4</sub>)<sub>2</sub>·6H<sub>2</sub>O, NaClO<sub>4</sub>, Mg(ClO<sub>4</sub>)<sub>2</sub>, KClO<sub>4</sub>, Cr(ClO<sub>4</sub>)<sub>3</sub>·6H<sub>2</sub>O, Co(ClO<sub>4</sub>)<sub>2</sub>·6H<sub>2</sub>O, Cu(ClO<sub>4</sub>)<sub>2</sub>·6H<sub>2</sub>O and Ni(ClO<sub>4</sub>)<sub>2</sub>·6H<sub>2</sub>O, respectively. The anions (X) used in this study are all [Na]X salts. Metal ion and anion stock

solutions used during the spectrophotometric measurements and titrations were prepared with Milli-Q deionized water ( $R > 18 \text{ M}\Omega$ ).

For the quantitative titrations, the concentration of sensor-1 subunits in the nanoparticles water suspensions was evaluated from their absorbance using the  $\epsilon$  values of the corresponding compound in aqueous solution (**1**:  $\lambda = 243 \text{ nm}$ ,  $\epsilon = 1.73 \times 10^4 \text{ M}^{-1} \text{ cm}^{-1}$ ). The desired amount of such nanoparticle suspensions was then transferred to a volumetric flask and an aqueous solution was added to reach a final volume of 10 mL. Then the adsorption and emission spectra were recorded. The excitation wavelength was 320 nm. The same amount of fluorescent nanoparticles were suspended in the corresponding different concentration of metal ions or anions solution (10 mL), the emission spectra of the fluorescent nanoparticles suspension with different concentrations of  $\text{Zn}^{2+}$  (or  $\text{H}_2\text{PO}_4^-$ ) and other metal ion solutions ( $\text{Cd}^{2+}$ ,  $\text{Ag}^+$ ,  $\text{Pb}^{2+}$ ,  $\text{Hg}^{2+}$ ,  $\text{Na}^+$ ,  $\text{Mg}^{2+}$ ,  $\text{K}^+$ ,  $\text{Cr}^{3+}$ ,  $\text{Co}^{2+}$ ,  $\text{Cu}^{2+}$ ,  $\text{Ni}^{2+}$ ) [or other anions ( $\text{HCO}_3^-$ ,  $\text{F}^-$ ,  $\text{Br}^-$ ,  $\text{I}^-$ ,  $\text{NO}_3^-$ ,  $\text{CH}_3\text{COO}^-$ ,  $\text{SO}_4^{2-}$ )] were measured respectively. All the measurements were repeated three times and the general average was obtained.

### Regeneration of the SSN

The desired amount of fluorescent silica@sensor-1 nanoparticles suspensions ( $[\text{sensor-1}] = 1.2 \times 10^{-4} \text{ M}$ ) was equilibrated with 10 mL of aqueous solutions containing  $5.1 \times 10^{-3} \text{ M Zn}^{2+}$  at room temperature, and the emission spectra of the suspension were measured. The nanoparticles were treated with a solution of EDTA-2Na ( $1.0 \times 10^{-2} \text{ M}$ ) and then separated by centrifugation (10000 r/min) and washed with tris-HCl (0.01 M) solution (water, pH = 7.10). The regenerated fluorescent silica nanoparticles were suspended in the same volume (10 mL) of aqueous solutions containing the same concentration ( $5.1 \times 10^{-3} \text{ M}$ ) of zinc, and the emission spectra were carried out again.

### Application of fluorescent silica nanoparticles for fluorescent images intracellular $\text{Zn}^{2+}$ ( $\text{H}_2\text{PO}_4^-$ ) in HeLa cells

HeLa cells were seeded at  $2 \times 10^6$  cells in a 10 cm Petri dish and were cultured in DMEM containing 10% fetal bovine serum and penicillin/streptomycin at  $37^\circ\text{C}$  in 5%  $\text{CO}_2$  and 95% air. After 24 h of cell attachment, the cells were incubated with SSN ( $[\text{sensor-1}] = 42 \mu\text{M}$ ) for 30 min at  $37^\circ\text{C}$ . The SSN were then removed and the cells were washed twice with physiological saline solution (NaCl: 0.9%, wt%). SSN pretreated cells were then diluted with the addition of  $\text{Zn}(\text{ClO}_4)_2$  (50  $\mu\text{M}$ ) and incubated for another 0.5 h at  $37^\circ\text{C}$ . Then, the cells were washed with physiological saline solution three times for further testing.

The cells were incubated with DSSN ( $[\text{sensor-1}] = 40 \mu\text{M}$ ) for 30 min at  $37^\circ\text{C}$ . The DSSN were then removed and the cells were washed twice with PBS buffer (phosphate buffered saline). DSSN pretreated cells were then diluted with the addition of  $\text{Zn}(\text{ClO}_4)_2$  (40, 100, 700  $\mu\text{M}$ , respectively) and incubated for another 0.5 h at  $37^\circ\text{C}$ . Then, the cells were washed with PBS buffer three times for further testing.

The cells were incubated with the  $[\text{DSSN@Zn}^{2+}]$  complex ( $[\text{sensor-1}] = 45 \mu\text{M}$ ,  $[\text{Zn}^{2+}] = 1.5 \text{ mM}$ ) for 60 min at  $37^\circ\text{C}$ . The  $[\text{DSSN@Zn}^{2+}]$  complex was then removed and the cells were

washed twice with PBS buffer. The  $[\text{DSSN@Zn}^{2+}]$  complex pretreated cells were then diluted with the addition of  $\text{NaH}_2\text{PO}_4$  (600  $\mu\text{M}$ , respectively) and incubated for another 0.5 h at  $37^\circ\text{C}$ . Then, the cells were washed with PBS buffer three times for further testing.

## Results and discussion

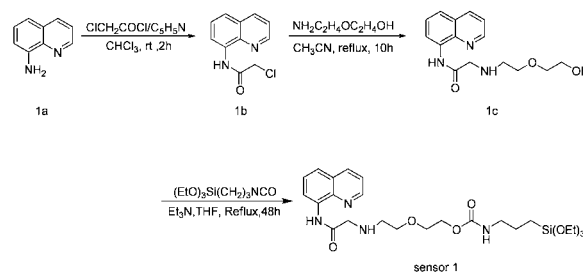
### Design of the fluorescent core-shell silica nanoparticles

In 1968, Stöber *et al.* described a pioneering synthesis method of nearly monodisperse silica nanoparticles *via* the hydrolysis and condensation of a silica alkoxide precursor (such as tetraethylorthosilicate, TEOS) in alcoholic solutions in the presence of aqueous ammonium hydroxide mixture.<sup>14</sup> This method is comparatively simple and both organic and inorganic dyes can be entrapped. To address the problem of sensor leakage in the silica backbone, Van Blaaderen *et al.* covalently linked fluorescein isothiocyanate (FITC) to 3-aminopropyltriethoxysilane and incorporated the dye into the silica matrix to obtain robust dye-rich silica nanoparticles.<sup>30</sup> After that, Kopelman, Rosenzweig and their co-workers proposed a new strategy for preparing fluorescent chemosensors within nanoparticles, dubbed PEBBLE sensors.<sup>19</sup>

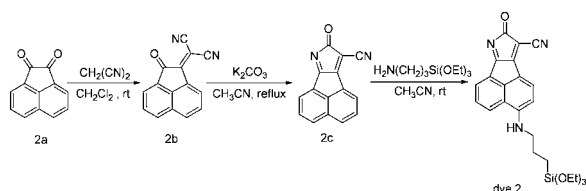
Here as depicted in Scheme 1, we synthesized a type of fluorescent sensor (DSSN) based on core-shell silica nanoparticles by a modified Stöber-Van Blaaderen method. The sensing systems were anchored onto the surface of the silica nanoparticles, to most extent, preserving the analytical characteristics of chemosensors and providing the large surface area for the sensor to interact with substrates. The reference dye **2** molecules were buried inside the silica matrix, which protected the dye from its surrounding environment, and the dye **2** just produced a reference signal for ratiometric measurements. On the other hand, metal-containing receptors could provide unsaturated coordination sites at the metal centers, and present some geometrical preference for anions of a given shape.<sup>31</sup> Therefore, the fluorescent silica nanoparticle  $[\text{DSSN@Zn}^{2+}]$  complex also could ratiometrically detect the anions in an aqueous solution with a high sensitivity.

### Chemical synthesis

We designed sensor **1** by chemically incorporating the fluoroionophore to the silica network *via* the reaction between the ethoxysilane groups of the fluoroionophore **1** and the silanol groups during hydrolysis and condensation of tetraethylorthosilicate. Synthesis of sensor **1** was depicted in Scheme 2. The



**Scheme 2** Synthesis of sensor **1**.



**Scheme 3** Synthesis of dye **2**.

compound 2-chloro-*N*-(quinolin-8-yl)-acetamide (**1b**) was prepared from 8-aminoquinoline (**1a**) and 2-chloroacetyl chloride in chloroform. Compound **1c** was obtained with 85.2% yield by reaction of eight equivalents of 2-(2-aminoethoxy) ethanol, *N,N*-diisopropylethylamine respectively with **1b** and KI (3 mol % based on **1b**) in acetonitrile. The reaction between compound **1c** and an equal equivalent of triethoxy(3-isocyanatopropyl)silane in anhydrous tetrahydrofuran afforded the fluorophore **1** as a yellow oil with a yield of 85.2%.

Dye **2** was derived from the fluorophore **2c**, which was structurally simple with strong long-wavelength emission and high fluorescence quantum yield.<sup>29</sup> As shown in Scheme 3, the starting material acenaphthalenequinone (**2a**) condensed with malononitrile to give the monoadduct **2b** with 97.3% yield. Following cyclization catalyzed by  $K_2CO_3$  in anhydrous acetonitrile, the precursor **2c** was obtained almost quantitatively. Then, at room temperature, the highly electron-deficient and highly reactive precursor **2c** reacted with 3-aminopropyltriethoxy silane in acetonitrile to give the fluorophore **2** with 15.1% yield.

### Preparation and characterization of fluorescent core-shell silica nanoparticles

The core-shell architecture of the three different fluorescent silica nanoparticles was synthesized *via* a modified Stöber-Van Blaaderen method. As depicted in Fig. 1, the silica core was synthesized by a pure silica precursor, tetraethoxysilane (TEOS), catalyzed by concentrated aqueous ammonia in an ethanolic solution. Following the synthesis of these core particles, the sensor **1**, was hydrolyzed with 0.405 mmol of TEOS to form the sensor layer. Finally, the as-synthesized silica@sensor-**1** nanoparticles (SSN) were centrifuged and resuspended repeatedly in deionized water, 70% ethanol solution and finally deionized water, in which they remain stable against flocculation, leaching, and degradation for months. Meanwhile, one kind of dye-**2**-rich core and silica shell nanoparticles (Fig. 1-i: DSN) were also prepared by hydrolyzing dye **2** in a basic ethanolic solution of TEOS to form dye-**2** rich core. Then a silica shell was hydrolyzed by pure silica precursor (TEOS). The dye-**2**@sensor-**1** nanoparticles (DSSN) were synthesized by a similar procedure (Scheme 1). The dye **2** was first hydrolyzed in basic ethanolic solution of TEOS to form a dye-**2**-rich core, then a silica layer was formed by the hydrolysis of a silica precursor (TEOS). After the reference dye-**2** was buried deep inside the nanoparticles, the sensor **1** precursor was hydrolyzed with TEOS to form the sensor layer.

The three different fluorescent silica nanoparticles were investigated with scanning electron microscopy (SEM) and transmission electron microscopy (TEM). As shown by SEM

and TEM, the as-prepared nanoparticles were uniformly monodispersed and separated from one another (Fig. 1-ii: a-f). These three kinds of nanoparticles almost have the same size (their final diameters of the as-prepared nanoparticles being  $71 \pm 6$  nm,  $70 \pm 8$  nm,  $69 \pm 9$  nm, respectively). Dynamic light scattering (DLS) data, shown in Fig. 2, showed a quite narrow size distribution centering at 80 nm. DLS hydrodynamic diameters are usually found to be slightly greater than those measured by TEM analysis. This may be attributed to the shrinkage of the particles due to the microscope electron beam.<sup>32</sup> From the DLS data, it was shown that the SSN and DSSN core-shell silica nanoparticles had a sensor-**1** rich shell of 16 and 17 nm, respectively. The core-shell silica nanoparticles were made from the same proportions of precursor materials. This indicated that the concentrations of dye **2** and sensor **1** covalently bound to the silica matrix were almost the same among SSN, DSN and DSSN.<sup>33</sup> Moreover, the binding of sensor **1** to the synthesized silica core was further proved by FT-IR (see the ESI,† Fig. S1) and fluorescent spectroscopy (Fig. 3).

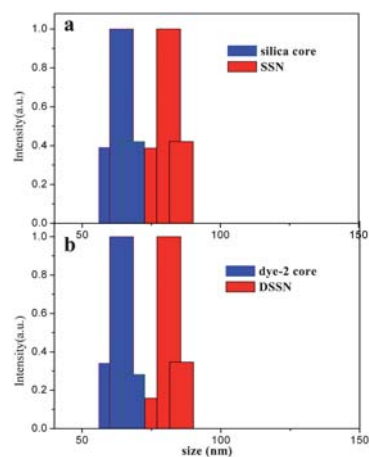


**Fig. 2** Dynamic light scattering (DLS) data of the core-shell architecture of two different fluorescent silica nanoparticles. (a) Size distribution of silica core and SSN nanoparticles; (b) Size distribution of dye-**2** core and DSSN nanoparticles.

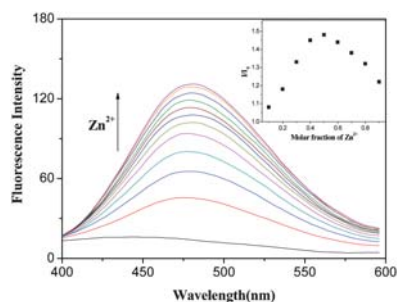


**Fig. 3** Emission spectra of a solution of SSN in the presence of increasing  $Zn^{2+}$  concentrations (0–1.0 mM) in tris-HCl (0.01 M) solution (water, pH = 7.10). (b). Inset: Job plot for SSN in tris-HCl (0.01 M) solution (water, pH = 7.10). The total [sensor-**1**] +  $[Zn^{2+}] = 100 \mu M$ . Conditions: [sensor-**1**] =  $3.1 \times 10^{-5}$  M,  $\lambda_{ex} = 320$  nm,  $\lambda_{em} = 482$  nm, 25 °C.

### SSN-based zinc detection

The signal response of SSN toward  $Zn^{2+}$  was measured at pH 7.10 (10 mM Tris-HCl solution, water) in both emission and absorption spectra (Fig. 3). Free SSN exhibited a weak fluorescence (quantum yield  $\Phi_0 = 0.005$ ). When  $Zn^{2+}$  was added to the SSN solution, a new absorption peak at 266 nm appeared, while the peak at 243 nm decreased, with an isosbestic point at 248 nm (ESI,† Fig. S2). The fluorescence intensity at 482 nm is significantly enhanced by approximately 13-fold (quantum yield,  $\Phi/\Phi_0 = 13.4$ ) with a 10 nm red-shift from 472 nm to 482 nm in fluorescence emission (Fig. 3). The Job plot (Fig. 3. inset) exhibited a maximum at 0.5 M fraction of  $Zn^{2+}$  in the solution of SSN, and indicated that a 1 : 1 complex was formed between the sensor-1 anchored onto the SSN and  $Zn^{2+}$ .

The selectivity of SSN towards  $Zn^{2+}$  was tested, as shown in Fig. 4. The SSN showed no fluorescence intensity changes for many metal ions such as  $Cd^{2+}$ ,  $Ag^+$ ,  $Pb^{2+}$ ,  $Hg^{2+}$ ,  $Na^+$ ,  $Mg^{2+}$ ,  $K^+$ ,  $Cr^{3+}$ ,  $Co^{2+}$ ,  $Cu^{2+}$  or  $Ni^{2+}$ . Under identical conditions, fluorescence intensity increased significantly in the presence of  $Zn^{2+}$ . The competition experiments for SSN were also conducted (Fig. 4). When the same amount of  $Zn^{2+}$  was added into the solution of SSN in the presence of other metal ions such as  $Cd^{2+}$ ,  $Ag^+$ ,  $Pb^{2+}$ ,  $Hg^{2+}$ ,  $Na^+$ ,  $Mg^{2+}$ ,  $K^+$ ,  $Cr^{3+}$ ,  $Ni^{2+}$ , no significant variation in the fluorescent intensity was observed by comparison with that  $Zn^{2+}$  only, whereas  $Co^{2+}$ ,  $Cu^{2+}$  quenched the fluorescence respectively. Moreover, an obviously blue-green emission of the SSN with  $Zn^{2+}$  solution can easily be observed by the naked eye (ESI,† Fig. S3). The results were in line with the ability of reported sensor **1c**<sup>28</sup> to selectively detect  $Zn^{2+}$  ions with no interferences from other metal ions.

### Application of SSN in cells

The taking up of molecules by cells is often facilitated by specific binding between these species and membrane-bound receptors (e.g. LDL or transferrin receptors). It is known that silica particles have a great affinity for the head-groups of a variety of

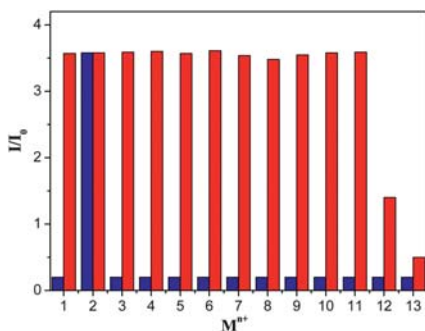


**Fig. 4** Fluorescence response of SSN in tris-HCl (0.01 M) solution (water, pH = 7.10) with different metal ions. Blue bars represent the response of SSN in the presence of the appropriate metal ion of interest. Red bars represent the response upon addition of  $Zn^{2+}$  ( $1.5 \times 10^{-4}$  M) to a solution of SSN and the appropriate metal ion of interest.  $I_0$  corresponds to the emission intensity of SSN without cation. 1, none; 2,  $Zn^{2+}$ ; 3,  $Na^+$ ; 4,  $Mg^{2+}$ ; 5,  $Pb^{2+}$ ; 6,  $Cd^{2+}$ ; 7,  $Ag^+$ ; 8,  $Hg^{2+}$ ; 9,  $K^+$ ; 10,  $Cr^{3+}$ ; 11,  $Ni^{2+}$ ; 12,  $Co^{2+}$ ; 13,  $Cu^{2+}$ . Conditions: [sensor-1] =  $3.1 \times 10^{-5}$  M,  $\lambda_{ex} = 320$  nm,  $\lambda_{em} = 482$  nm, 25 °C.

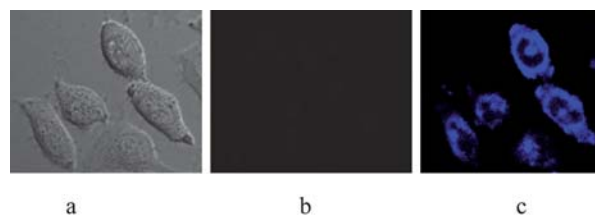


**Fig. 5** Fluorescence images of SSN ([sensor-1] =  $4.2 \times 10^{-5}$  M) induced by intracellular  $Zn^{2+}$  in HeLa cells. (a) Bright-field transmission image of HeLa Cells incubated with SSN. (b) Fluorescence image of HeLa cells incubated with SSN. (c) Fluorescence image of HeLa cells incubated with SSN for 30 min, washed three times, and then further incubated with  $5 \times 10^{-5}$  M  $Zn^{2+}$  for 30 min.

phospholipids.<sup>34</sup> Therefore, the silica particles' high affinity for cell surfaces by adsorption, which eventually leads to endocytosis is very convenient. We examined the application of SSN to cultured living cells (HeLa cells) by confocal spectral microscopy imaging system (CLSM). Incubation of HeLa cells with fluorescent silica nanoparticles for 0.5 h at 37 °C was followed by the addition of  $Zn^{2+}$  and then was incubated for another 0.5 h. The enhancement of fluorescence was observed (Fig. 5). The results suggest that SSN can penetrate the cell membrane and can be used for imaging  $Zn^{2+}$  in living cells.

### Regeneration of SSN

The reversibility of SSN was also investigated and the results were shown in Fig. 6. The stripping agent used in this experiment was a solution of EDTA-2Na. Fig. 6 showed a profile of fluorescence response of SSN during five sequential cycles. The whole process consisted of (1) adding the solution of EDTA-2Na to the [SSN@ $Zn^{2+}$ ] complex solution, (2) centrifuging the nanoparticles solution and washing the nanoparticles with tris-HCl (0.01 M) solution (water, pH = 7.10), and 3) sensing of  $Zn^{2+}$  ( $5.1 \times 10^{-3}$  M of  $Zn^{2+}$  in SSN solution ([sensor-1] =  $1.2 \times 10^{-4}$  M)). As shown in Fig. 6, SSN were able to re-combine with  $Zn^{2+}$  for at least four cycles, and the decrease in fluorescence intensity ( $I_5/I_1 = 87.1\%$ ) may be attributed to the stripping agent's effect on the sensing performance,<sup>35</sup> and a small amount of

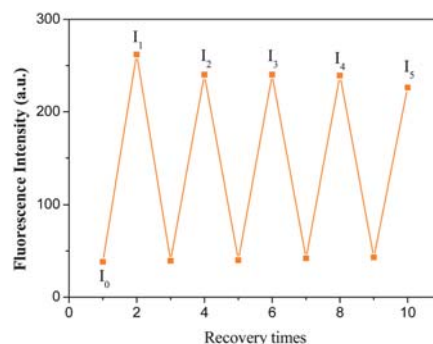


**Fig. 6** Reversibility of SSN ([sensor-1] =  $1.2 \times 10^{-4}$  M) response to  $Zn^{2+}$  ( $5.1 \times 10^{-3}$  M) over five complex/stripping cycles.  $I_0$  corresponds to the emission intensity of SSN without cation,  $I_1 \sim I_5$  corresponds to the emission of SSN with fresh zinc (II) solutions respectively. Conditions:  $\lambda_{ex} = 320$  nm,  $\lambda_{em} = 482$  nm, 25 °C.

agglomeration of the nanoparticles during multiple regeneration cycles was evidenced by a TEM image of the nanoparticles after the fifth time. However, **SSN** showed excellent reusability and stability towards  $\text{Zn}^{2+}$  within at least four successive cycles.

### DSSN-based zinc detection

As demonstrated by Kopelman and co-workers in the case of **PEBBLEs** sensors,<sup>19</sup> one of the main advantages of nanoparticle sensors is the possibility to convert a simple on-off or off-on chemosensor into a more valuable ratiometric one. This is done by embedding a second, substrate-insensitive dye within the particles which can produce a reference signal. To investigate this possibility, we chose the 8-oxo-8H-acenaphtho[1,2-b]pyrrol-9-carbonitrile derivative (dye **2**) as the inner reference. First, we prepared a class of dye-**2** rich core and pure silica shell fluorescent nanoparticles (**DSN**) of the same diameter as the **SSN** mentioned above. As the concentration of  $\text{Zn}^{2+}$  increased, there was little change in fluorescence intensity of the **DSN** solution (ESI,† Fig. S4). The results indicated that dye-**2** is indifferent to the substrates, and has the potential to produce a reference signal for ratiometric fluorescence detection. On the other hand, as shown in Fig. 7, the fluorescent intensity of **DSN** did not change at a wide pH range from 3 to 11, which is different from other fluorescent silica nanoparticles prepared by Rhodamine isothiocyanate (TRITC) or fluorescein isothiocyanate (FITC).<sup>36,37</sup> Furthermore, dye-**2** was structurally simple with strong long-wavelength emission and smaller molecules than other long-wavelength fluorophores, which decrease the aggregation when they were co-located into a single silica nanoparticle.<sup>33</sup> All the above advantages encouraged us to consider using dye-**2** as an inner reference to amplify the ratio of fluorescence intensity for the ratiometric measurements.

Therefore, we prepared dye-**2**-rich core and sensor-**1**-rich shell fluorescent silica nanoparticles (dye-**2**@silica@sensor-**1**, **DSSN**) (Scheme 1). The reference dye-**2** was buried deep inside the silica particles and further protected by a layer of silica. This layer of silica acted as a filter and protected the dyes from interactions with larger molecules such as proteins or organic quenchers that could interfere with the measurements.<sup>37</sup> A layer of sensor-**1** rich shell was attached to the surface of as-synthesized silica nanoparticles, which protects the reference dye while providing the

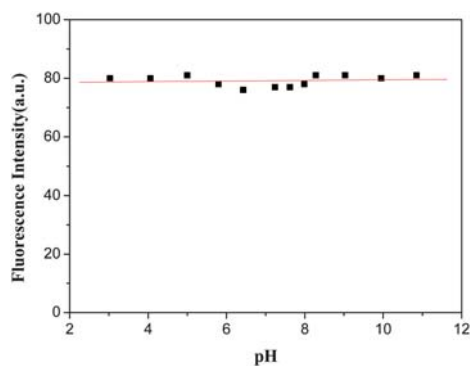


**Fig. 7** Dependence of the fluorescence intensity of **DSN** on pH in tris-HCl (0.01 M) solution (water, pH = 7.10). Conditions:  $\lambda_{\text{ex}} = 575 \text{ nm}$ ,  $\lambda_{\text{em}} = 591 \text{ nm}$ , 25 °C.

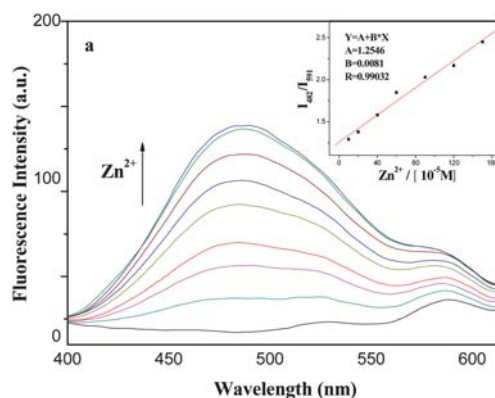


**Fig. 8** Emission spectra of a solution of dye-**2**-rich core and sensor-**1**-rich shell fluorescent silica nanoparticles (**DSSN**) in the presence of increasing  $\text{Zn}^{2+}$  concentrations (0–1.2 mM) in tris-HCl (0.01 M) solution (water, pH = 7.10). Inset: Ratiometric calibration curve  $I_{482 \text{ nm}}/I_{591 \text{ nm}}$  as a function of  $\text{Zn}^{2+}$  concentration (0.1–1.2 mM). Conditions: [sensor-**1**] =  $3.1 \times 10^{-5} \text{ M}$ ,  $\lambda_{\text{ex}} = 320 \text{ nm}$ ,  $\lambda_{\text{em1}} = 482 \text{ nm}$ ,  $\lambda_{\text{em2}} = 591 \text{ nm}$ , 25 °C.

greatest possible surface area for sensor interactions. As shown in Fig. 8, by adding the  $\text{Zn}^{2+}$  (0~1.5 mM) to the solution of **DSSN**, the fluorescence intensity at 482 nm (sensor-**1**@ $\text{Zn}^{2+}$ ) is significantly enhanced. There is another band at 591 nm (inner reference) which was marginally affected. The ratio of sensor-**1** to the dye-**2** was estimated as 62 : 1 by utilizing the fluorescence spectra (ESI,† Fig. S5, S6, Table S1). The inset in Fig. 8 shows the ratiometric calibration of fluorescence intensity of  $I_{482 \text{ nm}}/I_{591 \text{ nm}}$  corresponding to the concentration of  $0.1 \times 10^{-3} \sim 1.2 \times 10^{-3} \text{ M}$   $\text{Zn}^{2+}$ , which was in a linear manner with a correlation coefficient of  $R = 0.99032$ . This indicated that **DSSN** not only showed similar properties with **SSN** towards  $\text{Zn}^{2+}$  in aqueous solution (ESI,† Fig. S7), but can be potentially be used to quantitatively detect  $\text{Zn}^{2+}$  concentration in aqueous solutions by measuring the ratio of fluorescence intensity at two different wavelengths. Besides, a Job plot indicates a complex with 1 : 1 stoichiometry of the sensor-**1** anchored onto **DSSN** and  $\text{Zn}^{2+}$ , with the association constant of  $0.69 \times 10^4 \text{ M}^{-1}$ .<sup>38</sup>

### Application of DSSN in cells

To further demonstrate the **DSSN** with practical application potential, we applied it for ratiometric fluorescence imaging of  $\text{Zn}^{2+}$  in living cells. As shown in Fig. 5, the prepared fluorescent nanoparticles could penetrate the cell membrane for imaging  $\text{Zn}^{2+}$  in living cells. We changed the intracellular concentration  $\text{Zn}^{2+}$  by processing a series of paralleled experiments. The **DSSN** were incubated at 37 °C and washed thoroughly with PBS buffer to remove the extracellular nanoparticles. Then with the addition of  $\text{Zn}^{2+}$  with different concentrations, the living cells were incubated for another 0.5 h. The changes of the fluorescent intensity were measured using an inverted fluorescence microscope. ImageJ software gave an average emission value of the fluorescent photos. From the images we could see that free **DSSN** in living cells showed very weak fluorescence (ESI,† Fig. S8: blue, A2, B2, C2). With the increase of  $\text{Zn}^{2+}$  concentration, the fluorescence from 430 nm to 510 nm increased clearly (ESI,† Fig. S8: blue, A3, B3, C3), and the fluorescence from 570 nm to 650 nm

was shown as an inner reference signal (ESI,† Fig. S8: red, A4, B4, C4). The ratio of fluorescence at different wavelengths (blue/red) corresponding to different  $\text{Zn}^{2+}$  concentrations (ESI,† Fig. S9) indicated that **DSSN** could act as reliable zinc concentration indicators within living cells.<sup>22</sup> Furthermore, with the addition of an excess amount of EDTA in living cells which were intracellularly stained with **DSSN** and  $\text{Zn}^{2+}$ , the fluorescence was quenched, which implied the **DSSN** could reversibly detect  $\text{Zn}^{2+}$  (ESI,† Fig. S8: blue, A5, B5, C5).

### The $[\text{DSSN@Zn}^{2+}]$ complex-based $\text{H}_2\text{PO}_4^-$ detection

It is reported that metal-containing receptors can provide unsaturated coordination sites at the metal centers and present some geometrical preference for anions of a given shape, and metal–ligand receptors have a stronger affinity for anions in pure water at physiological pH value.<sup>39</sup> Based on this strategy, a variety of zinc-based phosphate anions receptors have been developed in the past few years.<sup>26,27</sup> The  $[\text{DSSN@Zn}^{2+}]$  complex's ability to ratiometrically detect anions and other species is of particular interest.

We prepared the  $[\text{DSSN@Zn}^{2+}]$  complex ( $[\text{sensor-1}] = 3.1 \times 10^{-5} \text{ M}$ ) by centrifuging the nanoparticles which bound the  $\text{Zn}^{2+}$  from zinc-rich solution (2.0 mM) and resuspended in tris-HCl (0.01 M) solution (water, pH = 7.10) for  $\text{H}_2\text{PO}_4^-$  detection. The results were shown in Fig. 9a. The addition of  $\text{H}_2\text{PO}_4^-$  to the aqueous solution of the  $[\text{DSSN@Zn}^{2+}]$  complex induced a dramatic fluorescence quenching effect on the band 482 nm, while the band of 591 nm was marginally affected. The decrease in fluorescence intensity on the band 482 nm may result from the

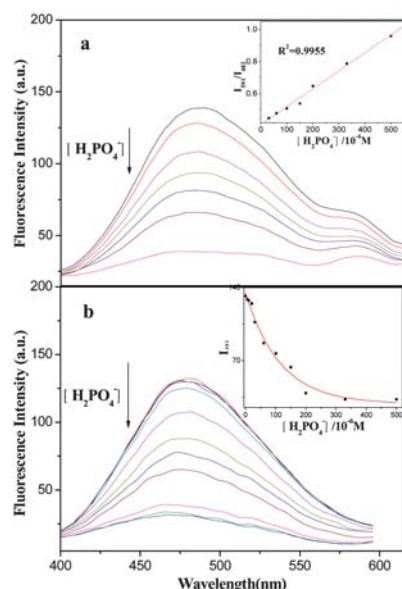


**Fig. 9** Fluorescence emission changes of the core-shell fluorescent silica nanoparticles  $[\text{DSSN@Zn}^{2+}]$  complex (a) and the  $[\text{SSN@Zn}^{2+}]$  complex (b) upon addition of  $\text{H}_2\text{PO}_4^-$  (6~500  $\mu\text{M}$ ) in tris-HCl (0.01 M) solution (water, pH = 7.10). (a) Inset: Ratiometric calibration curve  $I_{591 \text{ nm}}/I_{482 \text{ nm}}$  of complex  $[\text{DSSN@Zn}^{2+}]$  as a function of  $\text{H}_2\text{PO}_4^-$  concentration. (b) Inset: Titration curve  $I_{482 \text{ nm}}$  of complex  $[\text{SSN@Zn}^{2+}]$  as a function of  $\text{H}_2\text{PO}_4^-$  concentration. Conditions:  $[\text{sensor-1}] = 3.1 \times 10^{-5} \text{ M}$ ,  $\lambda_{\text{ex}} = 320 \text{ nm}$ ,  $\lambda_{\text{em1}} = 482 \text{ nm}$ ,  $\lambda_{\text{em2}} = 591 \text{ nm}$ , 25 °C.

regular indicator displacement assay between the  $[\text{DSSN@Zn}^{2+}]$  complex and  $\text{H}_2\text{PO}_4^-$ . Ratiometric calibration is shown in Fig. 9a (inset). It is observed that the ratio of fluorescence intensity of  $I_{591 \text{ nm}}/I_{482 \text{ nm}}$  corresponds to the concentration of  $\text{H}_2\text{PO}_4^-$  (50~500  $\mu\text{M}$ ) in a linear fashion (with a linearly dependent coefficient  $R^2$  of 0.9955). If the amount of  $\text{H}_2\text{PO}_4^-$  needed to decrease the initial fluorescence emission by 15% is taken as a reference detection limit, an anion concentration down to  $6.0 \times 10^{-6} \text{ M}$  was able to be measured, which is much lower than the reported phosphate anion receptors in water under physiological pH conditions.<sup>27</sup> On the other hand, the signal of  $[\text{SSN@Zn}^{2+}]$  complex towards  $\text{H}_2\text{PO}_4^-$  produced a quench at only one wavelength ( $\lambda_{\text{em}} = 482 \text{ nm}$ ) (Fig. 9b). The change of fluorescence intensity of  $I_{482 \text{ nm}}$  corresponding to the concentration of  $\text{H}_2\text{PO}_4^-$  could not be used as a standard curve for  $\text{H}_2\text{PO}_4^-$  quantitative detection (Fig. 9b inset). Therefore, the  $[\text{DSSN@Zn}^{2+}]$  complex can be potentially used to quantitatively and ratiometrically detect  $\text{H}_2\text{PO}_4^-$  concentration by measuring the fluorescence intensity at two different wavelengths compared with the  $[\text{SSN@Zn}^{2+}]$  complex.

It is well known that the luminescent properties exhibited by polynuclear d<sup>10</sup> (such as  $\text{Zn}^{2+}$ ,  $\text{Cd}^{2+}$ ) metal complexes are sensitive to structural and/or environmental changes.<sup>40</sup> So, the anion selectivity of the  $[\text{DSSN@Zn}^{2+}]$  complex was investigated among common anions such as monovalent ( $\text{H}_2\text{PO}_4^-$ ,  $\text{HCO}_3^-$ ,  $\text{F}^-$ ,  $\text{Br}^-$ ,  $\text{I}^-$ ,  $\text{NO}_3^-$  and  $\text{CH}_3\text{COO}^-$ ) as well as divalent ( $\text{SO}_4^{2-}$ ) anions in tris-HCl (0.01 M) aqueous solution at pH 7.10 at 25 °C. The fluorescence spectra of the aqueous solution of the  $[\text{DSSN@Zn}^{2+}]$  complex upon addition of these anions were recorded. As shown in Fig. 10, the addition of  $\text{H}_2\text{PO}_4^-$  (500  $\mu\text{M}$ ) to an aqueous solution of  $[\text{DSSN@Zn}^{2+}]$  complex ( $[\text{sensor-1}] = 3.1 \times 10^{-5} \text{ M}$ ) induced a dramatic fluorescence quenching at the wavelength of 482 nm; under the same conditions, anions such as  $\text{HCO}_3^-$ ,  $\text{F}^-$ ,  $\text{Br}^-$ ,  $\text{I}^-$ ,  $\text{NO}_3^-$ ,  $\text{CH}_3\text{COO}^-$  and  $\text{SO}_4^{2-}$  caused nearly no fluorescence intensity changes.

We further demonstrated the application of the  $[\text{DSSN@Zn}^{2+}]$  complex to cultured living cells by fluorescence microscopy (Fig. 11). Incubation of HeLa cells with the  $[\text{DSSN@Zn}^{2+}]$  complex for 1.0 h at 37 °C was followed by the addition of  $\text{H}_2\text{PO}_4^-$  and then was incubated for another 0.5 h. With the increase of the concentrations of  $\text{H}_2\text{PO}_4^-$ , the fluorescence from 430 nm to 510 nm was decreased (Fig. 11 blue: A2, B2). And the

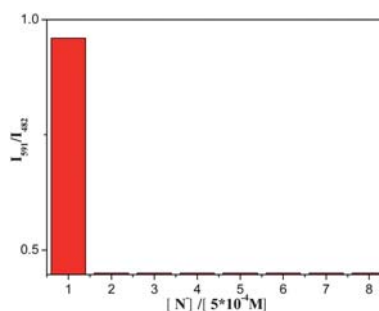


**Fig. 10** Fluorescence response of the  $[\text{DSSN@Zn}^{2+}]$  complex ( $[\text{sensor-1}] = 3.1 \times 10^{-5} \text{ M}$ ) in tris-HCl (0.01 M) solution (water, pH = 7.10) with different anions. 1,  $\text{H}_2\text{PO}_4^-$ ; 2,  $\text{Cl}^-$ ; 3,  $\text{F}^-$ ; 4,  $\text{Br}^-$ ; 5,  $\text{I}^-$ ; 6,  $\text{SO}_4^{2-}$ ; 7,  $\text{CH}_3\text{COO}^-$ ; 8,  $\text{NO}_3^-$ . Conditions:  $[\text{sensor-1}] = 3.1 \times 10^{-5} \text{ M}$ ,  $\lambda_{\text{ex}} = 320 \text{ nm}$ ,  $\lambda_{\text{em1}} = 482 \text{ nm}$ ,  $\lambda_{\text{em2}} = 591 \text{ nm}$ , 25 °C.

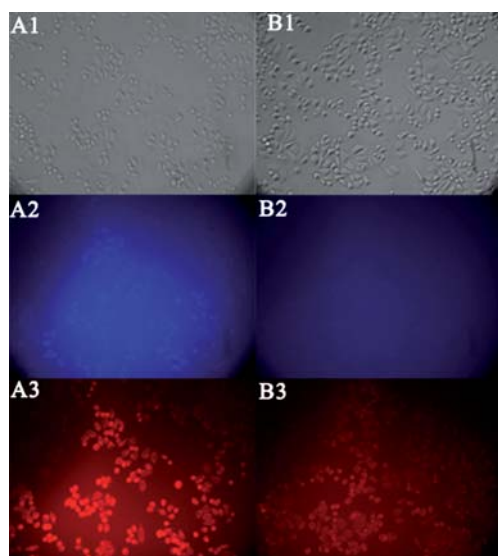


**Fig. 11** Fluorescence images of the  $[\text{DSSN@Zn}^{2+}]$  complex ( $[\text{sensor-1}] = 4.5 \times 10^{-5} \text{ M}$ ,  $[\text{Zn}^{2+}] = 1.5 \times 10^{-3} \text{ M}$ ) induced by intracellular  $\text{H}_2\text{PO}_4^-$  in HeLa cells. (A) Image of HeLa Cells incubated with the  $[\text{DSSN@Zn}^{2+}]$  complex (A1: Bright-field transmission image; Blue A2: Fluorescence image collected at 430~510 nm; Red A3: Fluorescence image collected at 570~650 nm); (B) Image of HeLa Cells incubated with the  $[\text{DSSN@Zn}^{2+}]$  complex for 60 min, washed three times with PBS, and then further incubated with  $6 \times 10^{-4} \text{ M H}_2\text{PO}_4^-$  for 30 min (A1: Bright-field transmission image; Blue B2: Fluorescence image collected at 430~510 nm; Red B3: Fluorescence image collected at 570~650 nm).

fluorescence from 570 nm to 650 nm could be used as an inner reference signal for ratiometric imaging  $\text{H}_2\text{PO}_4^-$  in living cells (Fig. 11 red: A3, B3).

## Conclusions

In conclusion, we have synthesized three kinds of novel core-shell fluorescent silica nanoparticles based on a modified Stöber-Van Blaaderen method. The SSN showed high selectivity toward  $\text{Zn}^{2+}$ , and can be reused to detect  $\text{Zn}^{2+}$  in aqueous solution and living cells. With dye-2 as an inner reference, the DSSN showed ratiometric fluorescent sensing properties toward  $\text{Zn}^{2+}$  in aqueous solution and living cell. Among common anions, such as  $\text{H}_2\text{PO}_4^-$ ,  $\text{HCO}_3^-$ ,  $\text{F}^-$ ,  $\text{Br}^-$ ,  $\text{I}^-$ ,  $\text{NO}_3^-$ ,  $\text{CH}_3\text{COO}^-$  and  $\text{SO}_4^{2-}$ , the  $[\text{DSSN@Zn}^{2+}]$  complex specifically responded to  $\text{H}_2\text{PO}_4^-$  in tris-HCl (0.01 M) aqueous solution at neutral condition. The ratio of fluorescence intensity linearly increased in the range 6~500  $\mu\text{M}$  of  $\text{H}_2\text{PO}_4^-$ . So it can be potentially used for quantification of  $\text{H}_2\text{PO}_4^-$  in aqueous solution at physiological pH conditions. We believe that alteration of common changes in fluorescence intensity (fluorescence quenching or enhancement) to ratiometric measurements by fabricating a class of core-shell nanomaterials is a very promising route to improve the detection properties of chemosensors for targets in aqueous solution. In addition, DSN as a new class of highly fluorescent and photostable core-shell silica nanoparticles, has the potential to be a fluorescent labeling agent for selectively tagging a wide range of biomedical targets, such as bacteria, cancer cells and individual biomolecules.

## Acknowledgements

The authors are grateful for the financial support from National Natural Science Foundation of China (Grants 90713026, 21076077), Science and Technology Foundation of Shanghai (Grants 073919109), the Key New Drug Creation and Manufacturing Program (Grants 2009ZX09103-102) and the Shanghai Leading Academic Discipline Project (B507). We also thank Dr Jinbiao Tu for the improvements of this paper.

## References

- 1 K. Rurack and U. Resch-Genger, *Chem. Soc. Rev.*, 2002, **31**, 116; A. P. d. Silva, H. Q. N. Gunaratne, T. Gunnlaugsson, A. J. M. Huxley, C. P. McCoy, J. T. Rademacher and T. E. Rice, *Chem. Rev.*, 1997, **97**, 1515; L. Prodi, *New J. Chem.*, 2005, **29**, 20.
- 2 C. D. Geddes and J. R. Lakowicz, *Topics in Fluorescence Spectroscopy*, Vol. 9, Springer, New York, 2005; A. W. Czarnik, *Fluorescent Chemosensors for Ion and Molecule Recognition*, American Chemical Society, Washington, DC, 1993.
- 3 G. J. Mohr, I. Klimant, U. E. Spichiger-Keller and O. S. Wolfbeis, *Anal. Chem.*, 2001, **73**, 1053; H. Fu, B. H. Loo, D. Xiao, R. Xie, X. Ji, J. Yao, B. Zhang and L. Zhang, *Angew. Chem., Int. Ed.*, 2002, **41**, 962; J. Raker and T. E. Glass, *J. Org. Chem.*, 2002, **67**, 6113; H. Takakusa, K. Kikuchi, Y. Urano, S. Sakamoto, K. Yamaguchi and T. Nagano, *J. Am. Chem. Soc.*, 2002, **124**, 1653; Y. Kubo, M. Yamamoto, M. Ikeda, M. Takeuchi, S. Shinkai, S. Yamaguchi and K. Tamao, *Angew. Chem., Int. Ed.*, 2003, **42**, 2036.
- 4 M.-C. Daniel and D. Astruc, *Chem. Rev.*, 2003, **104**, 293; R. Sardar, A. M. Funston, P. Mulvaney and R. W. Murray, *Langmuir*, 2009, **25**, 13840.
- 5 F. Pinaud, X. Michalet, L. A. Bentolila, J. M. Tsay, S. Doose, J. J. Li, G. Iyer and S. Weiss, *Biomaterials*, 2006, **27**, 1679; F. M. Raymo and I. Yildiz, *Phys. Chem. Chem. Phys.*, 2007, **9**, 2036.
- 6 T. Steinkamp and U. Karst, *Anal. Bioanal. Chem.*, 2004, **380**, 24.
- 7 M. Qhobosheane, S. Santra, P. Zhang and W. Tan, *Analyst*, 2001, **126**, 1274; Y. H. Jin, A. Z. Li, S. G. Hazelton, S. Liang, C. L. John, P. D. Selid, D. T. Pierce and J. X. Zhao, *Coord. Chem. Rev.*, 2009, **253**, 2998.
- 8 B. J. Melde, B. J. Johnson and P. T. Charles, *Sensors*, 2008, **8**, 5202.
- 9 J. Yan, M. C. Estévez, J. E. Smith, K. Wang, X. He, L. Wang and W. Tan, *Nanotoday*, 2007, **2**, 44; L. Wang, K. Wang, S. Santra, X. Zhao, L. R. Hilliard, J. E. Smith, Y. Wu and W. Tan, *Anal. Chem.*, 2006, **1**, 647; G. Yao, L. Wang, Y. Wu, J. Smith, J. Xu, W. Zhao, E. Lee and W. Tan, *Anal. Bioanal. Chem.*, 2006, **385**, 518.
- 10 J. M. Rosenholm, A. Meinander, E. Peuhu and Rasmus, *ACS Nano*, 2009, **3**, 197; K. Park, S. Lee, E. Kang, K. Kim, K. Choi and I. C. Kwon, *Adv. Funct. Mater.*, 2009, **19**; R. Kumar, I. Roy, T. Y. Ohulchanskyy, L. N. Goswami, A. C. Bonoio, E. J. Bergey, K. M. Trampusch, A. Maitra and P. N. Prasad, *ACS Nano*, 2008, **2**, 449; S. Santra, *Methods Mol. Biol.*, 2010, **624**, 151.
- 11 M. Liong, S. Angelos, E. Choi, K. Patel, F. Stoddart and J. I. Zink, *J. Mater. Chem.*, 2009, **19**, 6251; T. Y. Ohulchanskyy, I. Roy, L. N. Goswami, Y. Chen, E. J. Bergey, R. K. Pandey, A. R. Oseroff and P. N. Prasad, *Nano Lett.*, 2007, **7**, 2835; I. I. Slowing, J. L. Vivero-Escoto, C.-W. Wu and V. S.-Y. Lin, *Adv. Drug Delivery Rev.*, 2008, **60**, 1278.
- 12 P. Tallury, K. Payton and S. Santra, *Nanomedicine*, 2008, **3**, 579.
- 13 D. J. Bharali, I. Klejbor, E. K. Stachowiak, P. Dutta, I. Roy, N. Kaur, E. J. Bergey, P. N. Prasad and M. K. Stachowiak, *Proc. Natl. Acad. Sci. U. S. A.*, 2005, **102**, 11539; I. Roy, T. Y. Ohulchanskyy, D. J. Bharali, H. E. Pudavar, R. A. Mistretta, N. Kaur and P. N. Prasad, *Proc. Natl. Acad. Sci. U. S. A.*, 2005, **102**, 279.
- 14 W. Stöber, A. Fink and E. Bohn, *J. Colloid Interface Sci.*, 1968, **26**, 62.
- 15 F. J. Arriagada and K. Osseo-Asare, *J. Colloid Interface Sci.*, 1999, **211**, 210.
- 16 X. He, J. Chen, K. Wang, D. Qin and W. Tan, *Talanta*, 2007, **72**, 1519; H. Ou, D. R. Larson, M. Srivastava, B. A. Baird, W. W. Webb and U. Wiesner, *Nano Lett.*, 2005, **5**, 113; E. Rampazzo, S. Bonacchi, M. Montalti, L. Prodi and N. Zaccheroni, *J. Am. Chem. Soc.*, 2007, **129**, 14251; C. L. Wu,

- J. Q. Hong, X. Q. Guo, C. B. Huang, J. P. Lai, J. S. Zheng, J. B. Chen, X. Mu and Y. B. Zhao, *Chem. Commun.*, 2008, 750.
- 17 M. Arduini, F. Mancin, P. Tecilla and U. Tonellato, *Langmuir*, 2007, **23**, 8632.
- 18 Y. Piao, A. Burns, J. Kim, U. Wiesner and T. Hyeon, *Adv. Funct. Mater.*, 2008, **18**, 1.
- 19 H. Xu, J. W. Aylott, R. Kopelman, T. J. Miller and M. A. Philbert, *Anal. Chem.*, 2001, **73**, 4124; Y.-E. L. Koo, Y. Cao, R. Kopelman, S. M. Koo, M. Brasuel and M. A. Philbert, *Anal. Chem.*, 2004, **76**, 2498.
- 20 E. Brasola, F. Mancin, E. Rampazzo, P. Tecilla and U. Tonellato, *Chem. Commun.*, 2003, 3026; M. Arduini, S. Marcuz, M. Montolli, E. Rampazzo, F. Mancin, S. Gross, L. Armelao, P. Tecilla and U. Tonellato, *Langmuir*, 2005, **21**, 9314; M. Montalti, L. Prodi and N. Zaccheroni, *J. Mater. Chem.*, 2005, **15**, 2810; E. Rampazzo, E. Brasola, S. Marcuz, F. Mancin, P. Tecilla and U. Tonellato, *J. Mater. Chem.*, 2005, **15**, 2687; P. Grandini, F. Mancin, P. Tecilla, P. Scrimin and U. Tonellato, *Angew. Chem., Int. Ed.*, 1999, **38**, 3061; L. Fabbri, M. Licchelli, F. Mancin, M. Pizzeghello, G. Rabaioli, A. Taglietti, P. Tecilla and U. Tonellato, *Chem.-Eur. J.*, 2002, **8**, 94; J. Zheng, C. Xiao, Q. Fei, M. Li, B. Wang, G. Feng, H. Yu, Y. Huan and Z. Song, *Nanotechnology*, 2010, **21**, 045501.
- 21 M. J. Ruedas-Rama and E. A. Hall, *Anal. Chem.*, 2008, **80**, 8260; P. Teoloto, E. Rampazzo, M. Arduini, F. Mancin, P. Tecilla and U. Tonellato, *Chem.-Eur. J.*, 2007, **13**, 2238; L. Gao, Y. Wang, J. Wang, L. Huang, L. Shi, X. Fan, Z. Zou, T. Yu, M. Zhu and Z. Li, *Inorg. Chem.*, 2006, **45**, 6844.
- 22 K. Sarkar, K. Dhara, M. Nandi, P. Roy, A. Bhaumik and P. Banerjee, *Adv. Funct. Mater.*, 2009, **19**, 223.
- 23 S. Zhang, F. Lü, L. Gao, L. Ding and Y. Fang, *Langmuir*, 2007, **23**, 1584; José V. Ros-Lis, R. Casásús, M. Comes, C. Coll, M. D. Marcos, R. Martínez-Mañez, F. Sancenón, J. Soto, P. Amorós, Jamal E. Haskouri, N. Garró and K. Rurack, *Chem.-Eur. J.*, 2008, **14**, 8267; E. Kim, H. E. Kim, S. J. Lee, S. S. Lee, M. L. Seo and J. H. Jung, *Chem. Commun.*, 2008, 3921; S. A. El-Safty, D. Prabhakaran, A. A. Ismail, H. Matsunaga and F. Mizukami, *Adv. Funct. Mater.*, 2007, **17**, 3731.
- 24 E. M. Nolan and S. J. Lippard, *Acc. Chem. Res.*, 2009, **42**, 193; N. C. Lim, H. C. Freake and C. Bruckner, *Chem.-Eur. J.*, 2005, **11**, 38; E. L. Que, D. W. Domaille and C. J. Chang, *Chem. Rev.*, 2008, **108**, 1517; W. Jiang, Q. Fu, H. Fan and W. Wang, *Chem. Commun.*, 2008, 259; P. Jiang and Z. Guo, *Coord. Chem. Rev.*, 2004, **248**, 205; K. Kikuchi, K. Komatsu and T. Nagano, *Curr. Opin. Chem. Biol.*, 2004, **8**, 182; K. R. Gee, Z.-L. Zhou, W.-J. Qian and R. Kennedy, *J. Am. Chem. Soc.*, 2002, **124**, 776; J. H. Weiss, S. L. Sensi and J. Y. Koh, *Trends Pharmacol. Sci.*, 2000, **21**, 395.
- 25 S. K. Kim, D. H. Lee, J.-I. Hong and J. Yoon, *Acc. Chem. Res.*, 2008, **42**, 23; D. H. Lee, S. Y. Kim and J.-I. Hong, *Angew. Chem., Int. Ed.*, 2004, **43**, 4777; Anna K. H. Hirsch, Felix R. Fischer and F. Diederich, *Angew. Chem., Int. Ed.*, 2007, **46**, 338; A. Nonaka, S. Horie, T. D. James and Y. Kubo, *Org. Biomol. Chem.*, 2008, **6**, 3621.
- 26 Q. Tan, L. Wang, L. Ma, H. Yu, J. Ding, Q. Liu, A. Xiao and G. Ren, *J. Phys. Chem. B*, 2008, **112**, 11171; J. Shao, H. Linb and H. Lin, *Talanta*, 2008, **77**, 273; S. K. Kim, D. Seo, S. J. Han, G. Son, I.-J. Lee, C. Lee, K. D.L. b and J. Yoon, *Tetrahedron*, 2008, **64**, 6402; C. Caltagirone, P. A. Gale, J. R. Hiscock, Simon J. Brooks, M. B. Hursthouse and M. E. Light, *Chem. Commun.*, 2008, 3007; Z. Chen, X. Wang, J. Chen, X. Yang, Y. Lia and Z. Guo, *New J. Chem.*, 2007, **31**, 357; X. Lin, X. Wu, Z. Xie and K.-Y. Wong, *Talanta*, 2006, **70**, 32; C.-F. Chen and Q.-Y. Chen, *New J. Chem.*, 2006, **30**, 143; J. Yoon, S. K. Kim, N. J. Singh, J. W. Lee, Y. J. Yang, K. Chellappan and K. S. Kim, *J. Org. Chem.*, 2004, **69**, 581; S. K. Kim, N. J. Singh, S. J. Kim, H. G. Kim, J. K. Kim, J. W. Lee, K. S. Kim and J. Yoon, *Org. Lett.*, 2003, **5**, 2083; A. Ojida, Y. Mito-oka, M.-a. Inoue and I. Hamachi, *J. Am. Chem. Soc.*, 2002, **124**, 6256.
- 27 J. Du, X. Y. Wang, M. Jia, T. J. Li, J. F. Mao and Z. J. Guo, *Inorg. Chem. Commun.*, 2008, **11**, 999; X.-h. Huang, Y.-b. He, C.-g. Hu and Z.-h. Chen, *Eur. J. Org. Chem.*, 2009, 1549.
- 28 Y. Zhang, X. Guo, W. Si, L. Jia and X. Qian, *Org. Lett.*, 2008, **10**, 473.
- 29 Y. Xiao, F. Liu, X. Qian and J. Cui, *Chem. Commun.*, 2005, 239.
- 30 A. Van Blaaderen, A. Imhof, W. Hage and A. Vrij, *Langmuir*, 1992, **8**, 1514; A. Van Blaaderen and A. Vrij, *Langmuir*, 1992, **8**, 2921.
- 31 P. D. Beer, *Acc. Chem. Res.*, 1998, **31**, 71.
- 32 A. van Blaaderen and A. P. M. Kentgens, *J. Non-Cryst. Solids*, 1992, **149**, 161; A. Van Blaaderen, J. Van Geest and A. Vrij, *J. Colloid Interface Sci.*, 1992, **154**, 481; A. van Blaaderen and A. Vrij, *J. Colloid Interface Sci.*, 1993, **156**, 1.
- 33 D. R. Larson, H. Ow, H. D. Vishwasrao, A. A. Heikal, U. Wiesner and W. W. Webb, *Chem. Mater.*, 2008, **20**, 2677.
- 34 S. Mornet, O. Lambert, E. Duguet and A. Brisson, *Nano Lett.*, 2005, **5**, 281.
- 35 A. Sayari, S. Hamoudi and Y. Yang, *Chem. Mater.*, 2005, **17**, 212.
- 36 S.-W. Ha, C. E. Camalier, G.R.B. Jr. and J.-K. Lee, *Chem. Commun.*, 2009, 2881; L. Wang, J. Lei and J. Zhang, *Chem. Commun.*, 2009, 2195; H. Shi, X. He, K. Wang, Y. Yuan, K. Deng, J. Chen and W. Tan, *Nanomed.: Nanotechnol., Biol. Med.*, 2007, **3**, 266.
- 37 A. Burns, P. Sengupta, T. Zedayko, B. Baird and U. Wiesner, *Small*, 2006, **2**, 723.
- 38 B. Valeur, J. Pouget and J. Bouson, *J. Phys. Chem.*, 1992, **96**, 6545; J. Bouson, J. Pouget and B. Valeur, *J. Phys. Chem.*, 1993, **97**, 4552.
- 39 P. D. Beer and E. J. Hayes, *Coord. Chem. Rev.*, 2003, **240**, 167; A. Moletti, C. Coluccini, D. Pasini and A. Taglietti, *Dalton Trans.*, 2007, 1588; A. Ojida, I. Takashima, T. Kohira, H. Nonaka and I. Hamachi, *J. Am. Chem. Soc.*, 2008, **130**, 12095; D. A. Jose, S. Mishra, A. Ghosh, A. Shrivastav, S. K. Mishra and A. Das, *Org. Lett.*, 2007, **9**, 1979; V. Amendola, G. Bergamaschi, A. Buttafava, L. Fabbri and E. Monzani, *J. Am. Chem. Soc.*, 2010, **132**, 147.
- 40 V. W.-W. Yam and K. K.-W. Lo, *Chem. Soc. Rev.*, 1999, **28**, 323; C.-M. Che and S.-W. Lai, *Coord. Chem. Rev.*, 2005, **249**, 1296.